Evidence for an Intermediate in Tau Filament Formation†

Carmen N. Chirita‡ and Jeff Kuret*,§

Biophysics Program and Department of Molecular and Cellular Biochemistry, The Ohio State University College of Medicine and Public Health, Columbus, Ohio 43210

Received November 13, 2003; Revised Manuscript Received December 11, 2003

ABSTRACT: Alzheimer's disease is defined in part by the intraneuronal accumulation of filaments comprised of the microtubule-associated protein tau. In vitro, fibrillization of full-length, unphosphorylated recombinant tau can be induced under near-physiological conditions by treatment with various agents, including anionic surfactants. Here we examine the pathway through which anionic surfactants promote tau fibrillization using a combination of electron microscopy and fluorescence spectroscopy. Protein and surfactant first interacted in solution to form micelles, which then provided negatively charged surfaces that accumulated tau aggregates. Surface aggregation of tau protein was followed by the time-dependent appearance of a thioflavin S reactive intermediate that accumulated over a period of hours. The intermediate was unstable in the absence of anionic surfaces, suggesting it was not filamentous. Fibrillization proceeded after intermediate formation with classic nucleation-dependent kinetics, consisting of lag phase followed by the exponential increase in filament lengths, followed by an equilibrium phase reached in approximately 24 h. The pathway did not require protein insertion into the micelle hydrophobic core or conformational change arising from mixed micelle formation, because anionic microspheres constructed from impermeable polystyrene were capable of qualitatively reproducing all aspects of the fibrillization reaction. It is proposed that the progression from amorphous aggregation through intermediate formation and fibrillization may underlie the activity of other inducers such as hyperphosphorylation and may be operative in vivo.

Aggregation of the microtubule-associated protein tau into filamentous lesions is a hallmark pathology of Alzheimer's disease (AD)[1] and other tauopathic neurodegenerative diseases (*1*). Although tau filaments isolated from postmortem tissue display disease-dependent gross morphology and tau isoform composition, they are thought to share the cross-β-sheet conformation typical of "amyloid" (*2*). As a result, they bind anionic dyes such as thioflavin S and thiazin red (*3*).

Filaments isolated from end-stage AD are particularly well characterized and consist of all six full-length tau isoforms extensively phosphorylated and organized into twisted paired helical filaments (PHFs) and nontwisted straight filaments (SFs) (*4*). But the folding pathway though which tau protein, which when isolated in solution exists as a natively unfolded monomer (*5*), assembles into filaments has been described only on the macroscopic level. Among the earliest changes observable in AD-derived tissue specimens is the formation of nonfibrillar cytoplasmic aggregates of hyperphosporylated tau (*6*, *7*). These amorphous aggregates, as well as the earliest detectable fibrillar tau aggregates, frequently appear associated with membranous intracellular structures, suggesting that membranes may participate in the tau folding pathway (*6*, *7*). Because the maturation of amorphous aggregates into neurofibrillary tangles correlates with cognitive impairment (*7*, *8*), clarifying the pathway through which these changes occur is of critical importance.

In living cells and brain tissue, tau protein has been estimated as comprising 0.025−0.25% of total protein (*9*, *10*). Assuming intracellular protein concentrations of ∼200 mg/mL (*11*) yields estimates of total intracellular tau levels of 1−10 μM. At these concentrations, purified recombinant tau isoforms do not detectably aggregate over days of incubation under physiological conditions. However, aggregation and fibrillization of tau protein can be greatly accelerated under near-physiological conditions in vitro by the addition of anionic surfactants (*12*). These agents, which are powerful inducers of β-sheet structure in many proteins (*13*−*15*), abruptly form micelles above a critical concentration in aqueous solution (*16*). Because fibrillization-inducing activity resides with the micelle, we have argued that the surface of cellular anionic membranes may supply a natural source of nucleating activity for intracellular proteins such as tau (*12*). Most importantly, these surfaces facilitate aggregation at physiological concentrations of tau. But the kinetic pathway through which this occurs and its relationship to other in vitro assembly paradigms are unknown.

Here we describe the sequence of events that accompany surfactant-induced tau fibrillization and provide evidence for the involvement of a partially folded intermediate, surface-bound nucleation, and unidirectional filament extension. The data suggest mechanisms potentially underlying the macroscopic changes accompanying lesion maturation in authentic AD tissue.

† This work was supported by National Institute of Health Grant AG14452 (to J.K.).

* To whom correspondence should be addressed. E-mail: kuret.3@osu.edu. Phone (614) 688-5899. Fax: (614) 292-5379.

‡ Biophysics Program.

§ Department of Molecular and Cellular Biochemistry.

[1] Abbreviations: AD, Alzheimer's disease; AA, arachidonic acid; CMC, critical micelle concentration; PHF, paired helical filament; SF, straight filament; ThS, thioflavin S; uteroglobin,[4−14] PRFAHVIENLL.

10.1021/bi036034b CCC: $27.50
Published on Web 01/22/2004

EXPERIMENTAL PROCEDURES

Materials. Recombinant histidine-tagged htau40 and α-synuclein were prepared as described previously (*17*, *18*). AD-derived PHFs prepared as in ref *19* were generously supplied by Dr. Lester I. Binder (Northwestern University Medical School, Chicago, IL). Arachidonic acid (AA) was obtained from Cayman Chemicals (Ann Arbor, MI) and stored at −80 °C under argon until used. Alkyl sulfate detergents (12, 18, and 20 carbons) were obtained from Mallinckrodt (Paris, KY), Lancaster Synthesis (Pelham, NH), and Research Plus (Bayonne, NJ), respectively, as sodium salts. Glutaraldehyde, uranyl acetate, and 300 mesh carbon-coated copper grids were from Electron Microscopy Sciences (Ft. Washington, PA). *N*-Phenyl-1-naphthylamine, ThS, protamine (grade IV from salmon), and histone (type II-A from calf thymus) were from Sigma (St. Louis, MO). Stocks of protamine and histone were made in water at 800 μM and used the same day. Carboxylate-conjugated polystyrene microspheres of defined nominal diameter and molecular area (a measure of surface charge density reported in units of $Å^2$/equiv) were obtained from Bangs Laboratories, Inc (Fishers, IN). Cationic colloidal gold (20 nm gold particles conjugated to poly(L-lysine) was from Ted Pella (Redding, CA).

Aggregation Assays. Under standard conditions, htau40 (4 μM) was incubated without agitation in assembly buffer (10 mM HEPES, pH 7.4, 100 mM NaCl, 5 mM dithiothreitol) at 37 °C for up to 168 h in the presence or absence of fibrillization inducers (AA, alkyl sulfate detergents, or carboxylate-modified polystyrene beads). All samples incubated for more than 24 h were kept under argon in parafilm-sealed tubes. Samples were processed for assay by electron microscopy as described below.

Electron Microscopy Assays. Aliquots of tau polymerization reactions were treated with 2% glutaraldehyde (final concentration), mounted on Formvar/carbon-coated 300 mesh grids, and negatively stained with 2% uranyl acetate as described previously (*12*, *20*). Random images were viewed in a Phillips CM 12 transmission electron microscope operated at 65 kV, captured on film at 8000−100 000-fold magnification, digitized at 600 dots-per-inch resolution, and imported into Optimas 6.5.1 for quantification of filament lengths and numbers (*20*). Individual filaments (defined as any object greater than 50 nm in its long axis with both ends visible in the field of view) were counted manually.

For colloidal gold labeling experiments, sample aliquots were processed as described above except that they were treated (1 h at 37 °C) with cationic gold (diluted 1:100 from stock in assembly buffer without DTT) in a humid chamber prior to uranyl acetate staining.

For freeze fracture analysis, aliquots of the polymerization reactions were quickly frozen onto gold "hats" in liquid ethane cooled by liquid nitrogen and then loaded into a precooled Balzer freeze etching system (BAF 400T; Balzer Corp., Hudson, NH). Frozen samples were fractured at −120 °C under vacuum (9×10^{-7} mbar) and shadowed with platinum at an angle of 45° and with carbon perpendicular to the samples. Samples were rotated as the carbon evaporated to yield a more even coating and then removed from the instrument and thawed. Replicas were floated off the samples into distilled water and then transferred to Clorox bleach and digested for 1 h. Replicas were subsequently rinsed several times with distilled water and were further digested in two changes of methanol, followed by 30 min in methanol/chloroform (13:87). Replicas were then placed on 300 mesh copper grids and visualized as above.

Thioflavin S Fluorescence Measurements. Tau (4 μM) was aggregated at 37 °C as described above except that the reactions contained 10 μM ThS. Resultant changes in fluorescence were monitored at $\lambda_{ex} = 440$ nm and $\lambda_{em} = 495$ nm in a FlexStation plate reader (Molecular Devices, Sunnyvale, CA) operated at sensitivity 10, high gain using black-matrix, clear-bottom 96-well isoplates (Wallac, Turku, Finland) sealed with transparent foil (NUNC; Denmark). Readings were made every 15 min after initiating reactions by addition of inducer and were corrected using protein-free control reactions.

For disaggregation studies, purified htau40 (4 μM) was preaggregated (3 h at room temperature) with AA (75 μM) as described above and then diluted 20-fold into assembly buffer containing ThS (2 μM) and either 4 μM htau40, 50 μM arachidonic acid, or no additions. ThS fluorescence was then followed over time with constant stirring.

CMC Measurements. CMC values for SDS were estimated at 37 °C using *N*-phenyl-1-naphthylamine as described previously (*12*, *18*), except that various concentrations of protamine, histone, α-synuclein, or htau40 were included with the samples. Detergent stock solutions were prepared in 1:1 water/2-propanol.

Analytical Methods. Dependence of detergent CMC on protein concentration was fit to the empirical Corrin−Harkins equation (*21*):

$$\log \mathrm{CMC} = -k_{\mathrm{CH}}(\log n) + b_{\mathrm{CH}} \tag{1}$$

where n is the molar concentration of protein or salt and k_{CH} and b_{CH} are constants. The slope of these curves, k_{CH}, approximates the proportion of detergent micelles that are ionized (*22*).

Sigmoidal reaction progress curves were fit to the sigmoidal logistic equation (*23*):

$$y = y_0 + \frac{A}{(1 + \mathrm{e}^{-k_{\mathrm{app}}(t - t_{50})})} \tag{2}$$

where y is total filament length (50 nm cutoff) measured at time t, y_0 is total filament length at time zero, t_{50} is time to 50% maximum fibrillization, A is the maximum total filament length at equilibrium, and k_{app} is the apparent first-order rate constant for fibril growth in units of time^{-1} (*24*). Lag times, defined as the time where the tangent to the point of maximum polymerization rate intersects the abscissa of the sigmoidal curve (*25*), were calculated as $t_{50} - (2/k_{app})$ (*24*).

Hyperbolic reaction progress and concentration dependence curves were fit to the rectangular hyperbola:

$$y = \frac{ax}{b - x} \tag{3}$$

where y is fluorescence or initial velocity determined at time or concentration x and constant b corresponds to x at 50% y_{max} (i.e., t_{50} or 50% maximum rate).

Initial rates were calculated from hyperbolic reaction progress curves by fitting the data to the polynomial series

$$y = \alpha + \beta t + \gamma t^2 + ... + \zeta t^6 \quad (4)$$

where y is fluorescence intensity at time t and the coefficient β approximates the initial rate (*26*).

Equivalents of microsphere surface charge were calculated from the equation

$$\text{equiv/bead} = (\pi \cdot d^2 10^2)/A \quad (5)$$

where d is bead diameter in nanometers, and A is molecular area in Å^2/equiv.

Filament length distributions were fit to the exponential equation

$$y = ae^{bx} \quad (6)$$

where y is the percentage of all filaments filling a bin of length interval x and b is a constant reported in units of length^{-1} ± 95% confidence interval.

Statistics. The proportions of filaments associated endwise with beads and of beads associated with filaments were estimated using the Wilson score method and reported ± 95% confidence limit (*27*).

RESULTS

CMC Depression Is Protein Concentration Dependent. Surfactant micelle stability reflects the balance between forces that promote (e.g., the hydrophobic effect mediated by alkyl chains) and oppose (e.g., electrostatic repulsion mediated by ionic headgroups) micellization (*16*). Thus, micelle stability, as reflected in CMC values, is sensitive to additives that modulate these interactions such as simple salts and proteins. To quantify the effect of tau on anionic micelle stability, the dependence of CMC depression on tau molar concentration was determined and compared to literature values for NaCl (*28*). The analysis also included α-synuclein, a protein with net negative charge at assay pH previously shown to depress CMC (*18*), literature values for uteroglobulin,[4−14] a hydrophobic undecapeptide of neutral net charge (*29*), and histone and protamine, two extremely basic proteins rich in clustered positive charge. The concentration dependence of CMC depression was linear for all experiments when plotted on double log axes (Figure 1), consistent with the empirical Corrin−Harkins treatment of counterion effects on CMC (eq 1; ref *21*). The slopes of these plots, which approximate both the proportion of micelle ionization and the degree of counterion binding (*22*), were similar (average slope = 0.59 ± 0.08; $n = 6$), indicating that there was little selectivity among protein counterions, regardless of isoelectric point or net charge. Significant differences in concentration dependence were apparent, however, with proteins being 5−7 orders of magnitude more potent than the simple salt NaCl on a molar basis. Only a portion of this difference could be ascribed to polyvalency, as the neutral peptide uteroglobulin,[4−14] with its two positive charges, was still 1000-fold more potent than NaCl. Normalizing concentrations for either net or mole percent positive charge tightened the potency distribution, but proteins were still at least 4 orders of magnitude more potent than NaCl. These data suggest that hydrophobic interactions between polypeptide and detergent make an important contribution to CMC depression and that as a result even amphoteric proteins with net negative charges such as α-synuclein strongly depress detergent CMC at low micromolar concentrations.

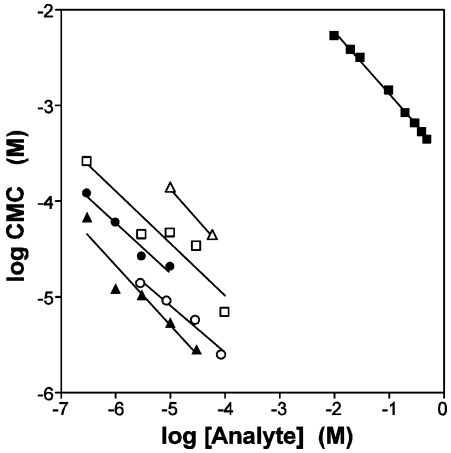

FIGURE 1: Corrin−Harkins analysis of analyte-mediated CMC depression. CMC values for SDS were determined in the presence α-synuclein (□; 0.3, 3, 10, 30, 100 μM), htau40 (●; 0.3, 1, 3, 10 μM), protamine (○; 3, 10, 30, 100 μM), and histone (▲; 0.3, 1, 3, 10, 30 μM), and plotted against protein concentration on double-logarithmic axes. Literature values for NaCl (■) and uteroglobin[4−14] (△) were plotted as well for comparison (*28*, *29*). Each line represents the least-squares fit of each data set to the empirical Corrin−Harkins equation (*21*) described in Experimental Procedures (eq 1). The data show that, regardless of net charge, proteins are powerful depressors of detergent CMC and far more potent than simple salts such as NaCl.

Micelles Serve as Nucleation Centers for Tau Fibrillization. When tau is incubated with preassembled anionic phospholipid vesicles, fibrillization proceeds from the vesicle surface, suggesting a key role for such surfaces in filament nucleation (*12*). However, it has been shown that when oppositely charged protein/surfactant pairs are coassembled, hierarchical structures more complicated than simple micelles or vesicles can form (*30*). To clarify the structural relationship between surfactant and tau in coassembly reactions, tau was fibrillized in the presence of AA and alkyl sulfate detergents ($C_{18}H_{37}NaSO_4$ and $C_{20}H_{41}NaSO_4$) and viewed by electron microscopy. These inducers were chosen because their long alkyl chains yield the largest micelles of any surfactants known to fibrillize tau in vitro (*31*). Low concentrations (<50 μM) of these agents yielded filaments with only a slight swelling seen at a few filament ends (data not shown). But micelle size is dependent on total surfactant concentration (*32*), and above 50 μM, these swellings became obvious for AA (Figure 2A), $C_{18}H_{37}NaSO_4$ (Figure 2B), and $C_{20}H_{41}NaSO_4$ (Figure 2C). Typically, swellings were seen at only one end of a filament (Figure 2A,C,D). They were not an artifact of negative staining, because they also could be seen in preparations analyzed by freeze fracture methods (Figure 2B). The swellings could correspond to detergent micelles, as predicted by the morphology of lipid vesicle-induced tau filaments (*12*), or to protein aggregates, as predicted by the micellar model of β-amyloid aggregation (*33*). To distinguish these possibilities, $C_{20}H_{41}NaSO_4$-induced tau filaments were stained with cationic colloidal 20-nm gold particles, which preferentially bind negatively charged surfaces such as those presented by anionic micelles (*34*). Resultant transmission electron micrographs showed intense staining of swellings, suggesting that they marked the location of detergent micelles that were preferentially local-

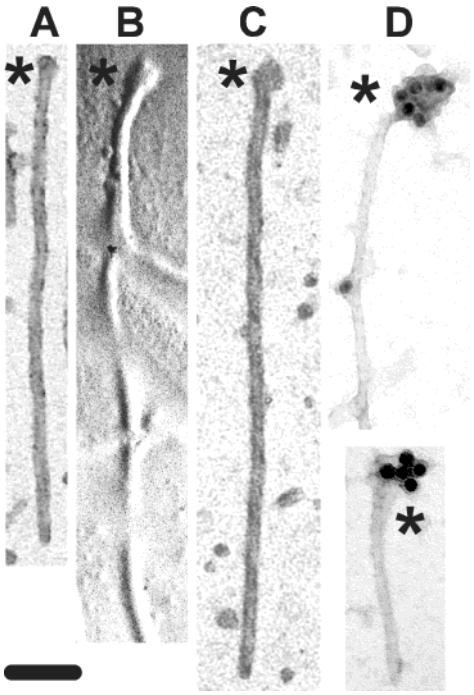

FIGURE 2: Anionic surfactants induce unidirectional tau filament growth. Htau40 (4 μM) was incubated (37 °C) in the presence of 50−100 μM (A) AA, (B) $C_{18}H_{37}NaSO_4$, or (C, D) $C_{20}H_{41}NaSO_4$ and then examined by negative stain (A, C, and D) or freeze fracture (B) transmission electron microscopy. In all cases, tau filaments were found extending from swellings located primarily at one filament end (∗). In panel D, swellings were selectively labeled with 20-nm cationic gold particles, suggesting that they contain concentrated anionic charge. Bar = 50 nm.

ized at one end of each filament (Figure 2D). These morphological findings are consistent with detergent aggregates formed in the presence of tau protein having energies of formation nearly identical to authentic micelles formed in buffer alone (*12*) and suggest that simple micelles are sufficient to induce tau fibrillization. Furthermore, these data suggest that micelles serve to nucleate tau fibrillization with subsequent endwise filament elongation occurring at only one actively growing end.

Anionic Surfaces Are Sufficient for Induction of Tau Fibrillization. The endwise association of tau filaments with micelles and vesicles suggested that their interactions were stable. In the case of fusogenic proteins such as β-amyloid peptide, stable interactions are mediated by partial insertion of protein into the hydrophobic core of vesicles (*35*). It has been proposed that protein aggregation follows and is dependent upon this insertion (*36*, *37*). To determine whether tau fibrillization required hydrophobic insertion, tau was incubated in the presence of carboxylate-modified polystyrene microspheres. These bodies, which are available in a wide variety of carboxylate substitution densities, are impermeable to proteins. Anionic microsphere lots were chosen on the basis of molecular areas roughly corresponding to values observed for surfactant Langmuir−Blodgett monolayers. These vary from ∼17−30 Å^2/equiv depending on the nature of the headgroup counterion (*38*, *39*). On the basis of measured aggregation numbers (*31*), however, micellar alkyl sulfate headgroup molecular areas may be as high as 60 Å^2/equiv. Therefore, microspheres with nominal molecular areas spanning the range 12−62 Å^2/equiv were employed for all experiments described below.

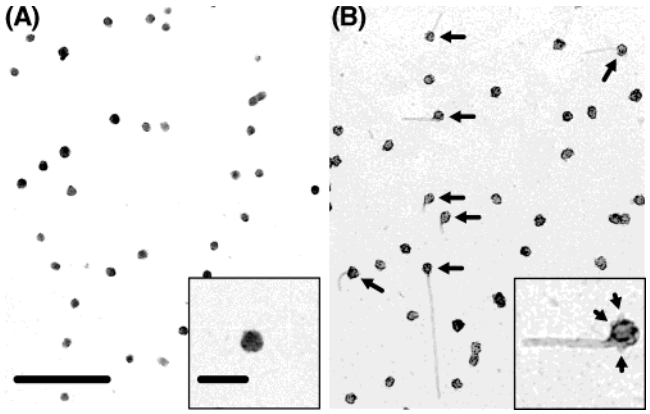

FIGURE 3: Induction of tau fibrillization using anionic microspheres. Carboxylate-substituted polystyrene microspheres (90 nm diameter, 12 Å^2/equiv molecular area; 591 pM) were incubated for 18 h at 37 °C with assembly buffer in the (A) absence or (B) presence of htau40 (4 μM) and then visualized by transmission electron microscopy. In the absence of protein, microspheres appeared as smooth-surfaced, roughly spherical objects without any associated filamentous material (A, inset). In contrast, incubation of microspheres in the presence of tau protein yielded rough surfaces that appeared enlarged relative to beads incubated in the absence of protein with ∼20% of microspheres having single filaments extending from their surfaces (arrows). Higher magnification (B, inset) revealed multiple short protrusions that may represent potential nucleation centers (arrowheads). Bar = 500 nm; inset bar = 100 nm.

In the absence of tau protein, microspheres (d = 90 nm; molecular area = 12 Å^2/equiv) incubated at 591 pM appeared in electron micrographs as spherical beads of roughly uniform dimension (Figure 3A). After 18 h in the presence of tau, however, filaments with identical morphology as those induced by AA, anionic detergents, and anionic lipids could be seen extending from a subpopulation of microsphere surfaces, nearly all filaments being microsphere-associated (Figure 3B). Closer inspection revealed that beads incubated in the presence of tau were larger than those incubated in its absence and that much of the difference stemmed from densely staining material on the bead surface (Figure 3B). Filaments appeared to grow out of this densely staining material. Although microspheres typically yielded only one mature filament per body, many had small (<10 nm) extensions on their surface with morphology similar to mature filaments (Figure 3B, inset). These data suggest that simple adsorption onto impermeable anionic surfaces is sufficient to nucleate tau fibrillization and that membrane penetration is not required.

Time Course of Microsphere-Mediated Tau Fibrillization. Because of their large uniform size and stability, microspheres offer the opportunity to visualize the nucleation and maturation of individual tau filaments. When the fibrillization of tau induced by 124 nM anionic microspheres (d = 90 nm; molecular area = 12 Å^2/equiv) was followed over 7 days by electron microscopy, total filament length was found to increase sigmoidally over time after a short period of absolute quiescence (Figure 4) with equilibrium attained in ∼24 h. Kinetic parameters of lag time and k_{app} were derived from fitting these data to a logistic curve as described in Experimental Procedures (eq 2). Under these conditions, lag time was 3.1 ± 0.5 h, t_{50} was 7.1 ± 0.4 h, and k_{app} was 0.5 ± 0.1 h^{-1}. Although no filamentous material >50 nm in length was detectable during the first 2 h of lag time (Figure

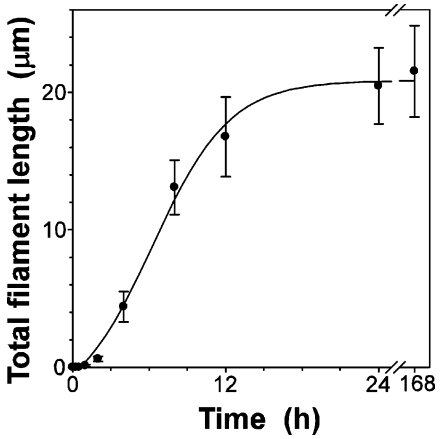

FIGURE 4: Time course of microsphere-mediated tau fibrillization. Htau40 (4μM) was incubated (37 °C) in assembly buffer in the presence of carboxylate-substituted polystyrene microspheres (90 nm diameter, 12 Å^2/equiv molecular area; 124 pM) for 7 days with aliquots removed and processed for transmission electron microscopy at the indicated time points. Each point represents the sum total length of all filaments >50 nm in length per field counted from 5 to 10 negatives at the indicated incubation time, whereas the solid line represents the best fit of all data points to a logistic regression (eq 2). Tau filament formation showed a clear lag phase, where no filaments were observed, followed by a phase of exponential increase, and ended in an equilibrium phase (achieved in ~24 h) after which further increases in filament length were not apparent.

4), accretion of the densely staining material on microsphere surfaces was apparent at the earliest time points (15 min). These data suggest that nucleation of tau fibrillization is a time-dependent process that occurs on the microsphere surface.

Tau Fibrillization Proceeds Through a ThS-Positive Intermediate. The addition of AA to solutions of tau produces an immediate increase in particulate material, visible by electron microscopy, paralleled exactly by changes in the fluorescence of ThS, a noncovalent probe for β-sheet structure (*20*). Because measurable fibrils (i.e., filaments >50 nm in length) appear to grow from this material, it has been suggested that the initial particulate material represents filament nuclei (*20*). However, the time course of fibrillization as determined by length measurements includes a distinct isoform-dependent lag time (*40*), suggesting that the particulate material and ThS fluorescence observed at early time points actually reflects formation of an assembly-competent intermediate (*41*). To clarify the temporal relationship between induction of ThS fluorescence and filament nucleation, the microsphere-induced tau aggregation time course described above was repeated in the presence of ThS. As with AA treatment, the addition of anionic microspheres induced an immediate increase in ThS fluorescence that continued hyperbolically over time (Figure 5A). Fitting these curves as rectangular hyperbolas (eq 3) showed that most (except the highest microsphere concentration tested) shared similar t_{50}'s, which averaged 1.7 ± 0.2 h (n = 7). These data show that the appearance of ThS fluorescence clearly precedes filament nucleation with nearly two-thirds of equilibrium fluorescence levels attained by the end of fibrillization lag time and with t_{50} for maximal fluorescence occurring 5.4 ± 0.7 h prior to the t_{50} for fibrillization. Moreover, they suggest the existence of a prefibrillar, ThS-positive intermediate that appears early in the reaction pathway.

ThS Fluorescence Changes Are Anionic-Charge-Dependent. Because of the stability of microspheres, it was possible to investigate the concentration dependence of ThS fluorescence change in greater detail than had been done previously with surfactant inducers such as AA. Like surfactant inducers, the dependence of induced ThS fluorescence on microsphere concentration (d = 90 nm; molecular area = 12 Å^2/equiv) was biphasic with a clear optimum visible at ~375 pM (Figure 5B). Well below this optimum, equilibrium fluorescence levels varied linearly with microsphere concentration. Yet despite the overall similarity in t_{50} for most microsphere concentrations, the initial rate of fluorescence change varied significantly and depended directly on microsphere concentration (Figure 5C). The concentration dependence of these initial rates fit a rectangular hyperbola (eq 3) with 50% maximum rate achieved at 370 ± 50 pM microspheres. These data suggested that the interaction between tau protein and anionic surfaces directly influenced the initial rate of formation of the ThS-positive intermediate and that the effect saturated at high microsphere/tau ratios.

To determine the influence of charge density on intermediate formation, the time course and concentration dependence of three microsphere preparations (diameter, molecular areas: 90 nm, 12 Å^2/equiv; 60 nm, 47 Å^2/equiv; 40 nm, 62 Å^2/equiv) was investigated. All three preparations induced ThS fluorescence with biphasic concentration dependence but with very different initial rates and optimal concentrations. Plots of optimal molar concentration of microspheres against their amount of surface charge were linear with slope equal to concentration of charge (Figure 6). Dependence of initial rates on charge concentration was linear as well (data not shown). These results suggest that the principal function of anionic surfaces early in the assembly pathway is to promote the formation of a ThS-positive, assembly-competent intermediate and that their potency in this regard is directly dependent on their anionic charge density.

The ThS-Positive Intermediate Is Metastable. The stability of the ThS intermediate formed by aggregating htau40 for 3 h at room temperature was examined. Under these conditions, most of the ThS fluorescence resulted from interaction with the intermediate (*41*). Rapid 20-fold dilution of the sample into assembly buffer alone with stirring dropped AA concentrations below the CMC and led to loss of ThS fluorescence with a first-order rate of 49.8 h^{-1} (Figure 7). Dilution into assembly buffer containing 2 μM htau40 (i.e., above the minimal concentration needed to support fibrillization; ref *42*) slowed the decay rate only modestly to 23.4 h^{-1}. In contrast, dilution into buffer containing 50 μM arachidonic acid (i.e., above the CMC) yielded a decay rate to 0.5 h^{-1}, 50-fold slower than dilution in buffer alone. These data show that ThS fluorescence is readily reversible and dependent on the presence of micelles for stability. For purposes of comparison, filament stability also was quantified using the electron microscopy assay. When diluted 20-fold into assembly buffer alone, total filament length did not change significantly (p < 0.05) over 90 min of incubation. Thus the intermediate detected by ThS is far less stable than filamentous tau and therefore is probably not fibrillar.

Origin of Exponential Length Distributions. In vitro fibrillization of tau with surfactants invariably produces

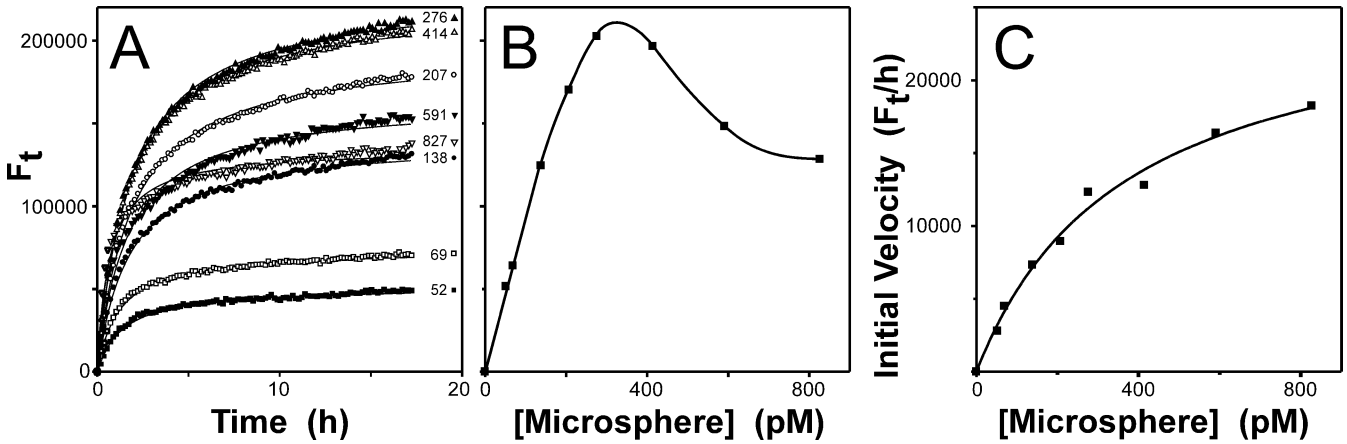

FIGURE 5: Time course of microsphere-mediated increases in ThS fluorescence. Aggregation of htau40 (4 μM) in the presence of varying concentrations of carboxylate-substituted polystyrene microspheres (90 nm diameter, 12 Å^2/equiv molecular area) was monitored using ThS (10 μM) fluorescence (F_t) as a function of time at 37 °C. In panel A, each point represents a fluorescence measurement, whereas each line represents the best nonlinear regression fit to a rectangular hyperbola (eq 3). Increasing concentrations of microspheres did not greatly change the half-time (t_{50}) of the reaction, which averaged 1.7 ± 0.2 h when microspheres were ≤591 pM. Panel B shows a replot of data in panel A, where each point corresponds to the final equilibrium fluorescence level at a given microsphere concentration. The biphasic concentration dependence resembled surfactant aggregation inducers such as AA (*20*). Panel C shows a replot of data in panel A, where each point represents the initial velocity of ThS fluorescence growth (F/h) at a given microsphere concentration (determined by fit of data in panel A to eq 4), and the line represents the best fit to a rectangular hyperbola (eq 3). The initial rate of ThS fluorescence growth depended on microsphere concentration and appeared saturable.

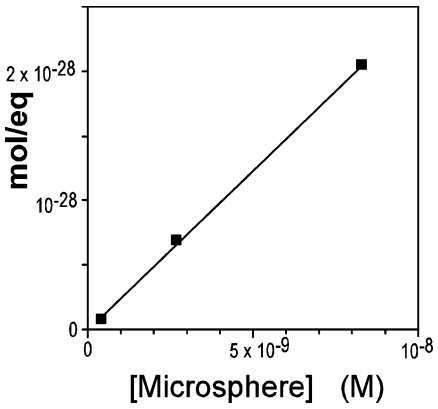

FIGURE 6: Anionic microsphere potency is directly proportional to surface charge. Aggregation of htau40 (4 μM) in the presence of varying concentrations of three carboxylate-substituted polystyrene microsphere preparations that differed in size and surface charge density (diameter, molecular areas: 90 nm, 12 Å^2/equiv; 60 nm, 46.7 Å^2/equiv; and 40 nm, 62.0 Å^2/equiv) was monitored using ThS (10 μM) fluorescence (F_t) as a function of time at 37 °C. Although the dependence of F_t on microsphere concentration was biphasic for each population, each microsphere population differed greatly in relative potency (data not shown). The figure shows a replot of these data, where each point represents the microsphere concentration yielding maximum F_t against the inverse amount of negative charge (mol/equiv; calculated from eq 5) of the three microsphere populations tested. The line represents linear regression analysis of the data points with slope equal to charge concentration (equiv/L). Charge concentration, rather than molecular area or microsphere size, is the principal determinant of potency with respect to ThS fluorescence.

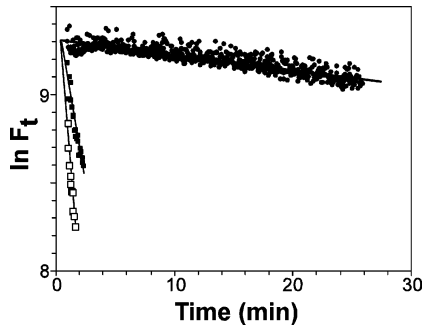

FIGURE 7: Disaggregation of synthetic tau filaments. Htau40 (4 μM) aggregated in the presence of assembly buffer containing AA (75 μM) and ThS (2 μM) for 3 h at room temperature was diluted 20-fold into assembly buffer containing ThS (2 μM) and either 4 μM htau40 (■), 50 μM arachidonic acid (●), or no additions (□). Each point represents ThS fluorescence (F_t) measured as a function of time after dilution, and the line is the best fit of the data points to a first-order decay. Stability of the ThS signal depended on the presence of AA.

exponential distributions of filament lengths (*12*, *43*). These may result from shear-dependent breakage during preparation, time-dependent nucleation, or energy distributions at equilibrium (*44*). To clarify this issue, the length distributions of filaments formed during incubation with anionic microspheres were calculated and plotted on a semilogarithmic scale. After 6 h of incubation, filament distributions were nearly exponential with most filaments (86.6% ± 2.8%) being microsphere-associated through one end (Figure 8). In contrast, only 13.6% ± 1.8% (n = 1314 observations) of microspheres had nucleated filaments >50 nm in length. The absence of significant numbers of isolated filaments rules out shearing as an influence on length distribution. Moreover, as shown previously with dithiothreitol as inducer (*45*), length distributions were exponential at the earliest measurable time points (4 h; data not shown), suggesting that equilibrium considerations also were not a factor. Rather, the data suggest that length distributions reflect the kinetic mechanism of assembly and arise from the exponential increase in filament length as a function of time.

For purposes of comparison, length distributions of authentic filaments purified from AD brain by two differential centrifugation-based methods (*19*, *46*) also were calculated. Both preparations adopted near-exponential length distributions with slope constants (b, calculated from eq 6) of −5.3 ± 0.2 and −2.7 ± 0.2 μm^{-1} (Figure 8). These closely paralleled values for synthetic filaments aggregated 3 h with AA (b = −5.4 ± 0.2 μm^{-1}; Figure 1 in ref 12) but

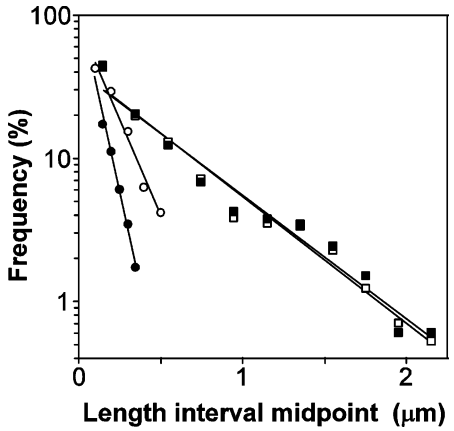

FIGURE 8: Microsphere-induced tau fibrillization yields exponential length distributions. Htau40 (4 μM) was incubated (6 h at 37 °C) in the presence of 124 pM carboxylate-substituted polystyrene microspheres (90 nm diameter, 12 Å^2/equiv molecular area), and then examined by transmission electron microscopy at 8000-fold magnification. The lengths of all filaments (□) ≥50 nm in length and also the filament subpopulation associated endwise with microspheres (■) were then measured from digitized images and plotted. Each data point represents the percentage of analyzed filaments (n = 664 and 575 for total and microsphere-associated populations, respectively) that segregated into consecutive length intervals (200-nm bins), whereas each line represents the best fit of data points to an exponential regression (eq 6). Under these conditions, 86.6% ± 2.8% of all measurable synthetic filaments were microsphere-associated with nearly identical percentages seen in individual bins. For comparison, the length distributions (50 nm bin size) of authentic AD-brain-derived tau filaments were calculated from the literature (Figure 1A of ref 46; n = 95; ●) and from freshly analyzed material (n = 140; ○) prepared as in ref *19*. Although their average lengths differ, both authentic tau filament preparations adopt an exponential length distribution.

were much shorter than those formed from microspheres (Figure 8; $b = -0.88 \pm 0.07$ μm^{-1}), presumably because the latter formed fewer nucleation centers over a longer period of time. Although purified filaments correspond to only a fraction of filamentous material in brain, their length distributions are consistent with time-dependent processes such as those described here underlying filament formation in disease.

DISCUSSION

Mechanism of AA-Mediated Tau Fibrillization. The above data suggest that induction of tau fibrillization with anionic surfactants such as AA proceeds by the following pathway. The first step involves binding of surfactant in dispersed form to natively unfolded tau protein. As with other polyelectrolytes (*47*), the initial interactions are likely electrostatic and result in accumulation of surfactant at sites along the tau molecule, eventually leading to cooperative and localized surfactant aggregation well below the CMC observed in the absence protein. The dependence of CMC depression on tau concentration as revealed by Corrin−Harkins plots suggests that while cationic interactions certainly influence micelle stabilization, hydrophobic interactions may also play a role. It has been shown that the combination of these interactions can not only reduce CMC but also effectively anchor polymers to individual micelles (*48*). A homogeneous solution of surfactant-bound tau protein is unlikely to result from these interactions. Rather, because micellization is highly cooperative and the number of interacting sites on tau is limited, tau protein is predicted to adopt a bimodal distribution consisting of surfactant bound and unbound populations (*49*). Computational models (*50*) and direct laboratory evidence (*51*) for such distributions have been reported in other systems. The proportion of tau that is surfactant-bound is predicted to increase as surfactant concentrations rise, until at saturation equilibrium shifts completely toward the micelle-bound state. As a result, lower quantities of unfolded tau are available to support intermolecular reactions such as filament nucleation and extension, giving rise to the biphasic surfactant dose response curve as competing intramolecular reactions (such as α-helix formation) predominate (*14*, *29*).

The association of surfactant micelles with tau protein initiates conformation changes that culminate in fibrillization and formation of cross-β-sheet structure (*2*). It has been argued that binding of surfactant in dispersed form is responsible for inducing β-sheet structure in many proteins of diverse primary structure including β_2-glycoprotein I (*13*) and complement receptor 1 derived peptide (*14*). But these studies did not appreciate the ability of protein to greatly lower surfactant CMC, and at least in the case of both tau and α-synuclein fibrillization, inducing activity actually resides with the micelle rather than dispersed surfactant (*12*, *18*). Results presented here show that conformational changes accompanying formation of the tau/surfactant mixed micelle do not necessarily form a template for addition of tau monomer. Rather, it is the creation of negatively charged micellar surface that plays the key role in the process. In fact, results with anionic microspheres suggest that no interaction between tau and inducer is necessary beyond simple adsorption, since these impermeable bodies promote fibrillization much like surfactants with respect to kinetics and biphasic potency. Consistent with this model, preformed lipid vesicles also nucleate tau filament formation (*12*). Therefore, the second step in the pathway appears to involve binding of the free tau population to the anionic surface, which leads to rapid formation of a ThS-positive intermediate without a lag period. The potency of anionic surfaces with respect to the initial rate of intermediate formation and the maximal extent of ThS fluorescence change is directly proportional to the concentration of negative charges. The ThS-sensitive intermediate is metastable; it relies on the presence of anionic surface for its existence. When surfactant is withdrawn, the intermediate rapidly disappears, suggesting it is not fibrillar (synthetic filaments are stable for at least 90 min after withdrawal of surfactant). Rather, ThS reactivity suggests that it represents a β-structure-containing species that can serve as a nucleation site in the folding pathway leading to fibrils. The intermediate does not appear to represent dimer, because dimerization alone does not yield ThS fluoresence (*41*). Micelle−tau interactions stabilize not only the intermediate but the entire micelle as well. As a result, micelles that normally have average lifetimes shorter than 1 s (*52*) survive for hours as tau-decorated structures, becoming visible in the electron microscope as small particles at early time points and swellings at the end of growing filaments later in the time course.

The final step in the pathway involves fibrillization. It follows classic nucleation-dependent kinetics, consisting of a nucleation phase characterized by a pronounced lag time, followed by an exponential growth phase characterized by

an apparent first-order growth rate, k_{app}, and then an equilibrium phase where further filament growth ceased (*53*). Typically, only one filament >50 nm in length matures per microsphere, although morphological evidence suggested that multiple nucleation events are possible. Assuming similar behavior for anionic surfactant micelles explains the differing length distributions and concentration dependencies measured for htau40 and AA, $C_{18}H_{37}NaSO_4$, and $C_{20}H_{41}NaSO_4$ (*12*). The number of filaments reflects the number of nucleation centers, which is proportional to the micelle concentration and thus dependent on the interplay between CMC and aggregation number (*54*):

$$m = (S_T - \mathrm{CMC})/N_a \quad (7)$$

where m is micelle concentration, S_T is total surfactant concentration, and N_a is the aggregation number. Up to the peak of its biphasic dose response curve, increasing micelle concentrations yield more nucleation centers and therefore more filaments that, at constant tau concentration, achieve shorter average lengths. Comparison among tau isoforms is more complicated, because these differ in the concentration dependence of nucleation as reflected in lag time (*40*).

Once nucleated, tau filaments grow unidirectionally from the inducer surface. The presence of only one actively growing end distinguishes the pathway described here from spontaneous aggregation pathways followed by other amyloids (*55*−*57*). At equilibrium, tau filaments remain associated with nucleation centers, explaining the substoichiometric recovery of AA with filaments (*12*). Previously, this observation was ascribed to transient association (*12*), but the work presented herein suggests that it derives from unidirectional elongation combined with stable association. The final length distribution of the filament population is exponential owing to the time-dependent nucleation event, as opposed to filament breakage or equilibrium considerations. Authentic AD-derived filaments also show exponential length distributions, suggesting that time-dependent nucleation events such as those described here may play a role in their formation. However, purified filaments represent only a portion of total filaments in AD lesions (*19*, *46*), and also the susceptibility of isolated filaments to shearing and breakage has been noted previously (*58*, *59*). Thus, estimates of the length distribution and number-average length of authentic filaments must be interpreted with caution.

Comparison with Other Fibrillization Inducers in Vitro. Anionic polyelectrolytes such as heparin induce tau fibrillization (*60*, *61*). These are generally weaker fibrillization inducers of full-length tau isoforms than surfactants in the sense that they require 10−100 μM tau concentrations to support measurable aggregation over a period of days (*62*). Nonetheless, heparin resembles AA with respect to its requirement for anionic charge (*61*), biphasic concentration dependence (*62*), ability to induce twisted morphology after days of incubation at physiological temperatures (*41*), and ability to generate ThS-reactive aggregates (*62*). It has been argued, however, that the aggregation pathway differs from that found here for surfactants by not proceeding through a ThS-positive intermediate (*41*, *63*). Indeed, the kinetic pathway through which a protein aggregates can be concentration-dependent (*64*). But heparin-induced fibrillization has never been quantified relative to the time course of ThS fluorescence, so the presence of an intermediate cannot be ruled out at present. It will be important to determine whether the mechanism outlined here is unique to anionic surfaces or can be extended to inducers having low molecular areas such as heparin.

The surfactant-induced tau fibrillization pathway also shares features with "surface-catalyzed" aggregation described for other amyloid-forming proteins (*65*, *66*). Common behavior includes the presence of anionic charge, dramatic acceleration of aggregation rate, presence of a pathway intermediate, tight association between mature filaments and the inducing surface, time-dependent rearrangement or heterogeneous nucleation to form twisted filaments, and what appears to be a decrease in the minimal concentration of protein required to support fibrillization at equilibrium. The latter phenomenon may result from changes in equilibria at filament ends (*18*) or among alternative pathways (*43*). The principal difference is that tau filaments induced by anionic surfaces extend out into solvent rather than growing along the surface. Referring to these surfaces as "catalysts" or "chaperones" may be inappropriate, however, since they remain associated with reaction products and do not appear to turn over. On the other hand, catalytic behavior may be claimed if a portion of the stabilized intermediate exists in solution and survives long enough to influence the equilibrium at growing filament ends (*18*).

Microspheres offer a convenient alternative for studying surface-mediated protein aggregation in vitro (*67*). They can be obtained with defined surface chemistry in uniform sizes that, unlike surfactant micelles, do not change with concentration or ionic strength (*68*). In contrast to mica slabs, their small diffusion boundary layer makes them especially suitable for kinetic studies (*69*). Moreover, they can facilitate observation of individual nucleation and extension events by electron microscopy owing to their easily identifiable profile. Because of their tight association with filaments, microspheres can provide an internal standard for quantitation of fibrillization, so in the future, it may be possible to normalize single electron micrographs to the entire reaction volume and therefore calibrate such data in terms of molar concentration.

Comparison with Tau Aggregation in AD. The proposed pathway of anionic surface-induced tau fibrillization parallels events detected in authentic tissue. Early events include the aggregation of tau protein into nonfibrillar deposits (*70*). This may result from hyperphosphorylation of tau, which can raise free intracellular tau concentrations by lowering tau−tubulin affinity (*71*, *72*) and promote amorphous aggregation in vitro (*73*, *74*). Aggregated phosphotau can rapidly form filaments at low ionic strength in vitro, although the relationship between this material and authentic filaments is not established (*75*). But in vivo, amorphous aggregates appear in conjunction with intracellular membranes (*6*, *7*), and it is here that the earliest fibrillization or at least β-conformation-enriched species are detectable using fluorescent dyes (*7*). Whereas some lesions develop predominantly SFs (*76*), late stage disease is dominated by PHF morphology, which may represent a minimal energy form (*77*). In vitro, the htau40 isoform used here initially forms untwisted filaments that correspond to a PHF hemifilament (*20*), but after a period of days, it adopts the mass per unit length of mature PHF (*78*). In end-stage disease, individual PHFs appear in endwise

association with membranes, consistent with surface-mediated nucleation and unidirectional extension from stable tau−membrane complexes (*79*). Together these data are consistent with an assembly pathway involving amorphous aggregation followed by fibrillization and suggest intermediate formation as the potential nexus between phosphorylation and anionic surfactant-induced pathways.

Pharmacological Implications. Certain members of the Congo red family of dyes inhibit the fibrillization of several proteins, including tau (*80*). The model presented here suggests that the prefibrillar intermediate may be the binding target for this class of inhibitors. The intermediate binds ThS with micromolar affinity (*20*), suggesting that it contains at least partially folded structure in β-sheet conformation. Although ThS itself is not inhibitory at 10 μM concentration (data not shown), other ligands may interact with the dye binding site so as to stabilize the intermediate and inhibit its participation in subsequent nucleation events. Stabilization of the intermediate could also raise the apparent minimal concentration of tau necessary to support filaments at equilibrium, potentially leading to disassembly of mature filaments before they become irreversibly cross-linked. Thus unlike the natively unfolded tau monomer, the partially folded intermediate may represent a tractable target for inhibitor design. The model predicts that inhibitory selectivity among amyloids may be achievable on the basis of assembly mechanism.

ACKNOWLEDGMENT

We thank Dr. Mike Zhu, Ohio State University Center for Molecular Neurobiology, for access to his fluorescence plate reader, and Profs. Lester I. Binder and Robert W. Berry, Northwestern University Medical School, for their generous gift of brain-derived tau filaments. We also thank Mihaela Necula and Erin Congdon for assistance with filament length measurements and Kathy Wolken for guidance in freeze fracture electron microscopy methods.

REFERENCES

1. Buee, L., Bussiere, T., Buee-Scherrer, V., Delacourte, A., and Hof, P. R. (2000) Tau protein isoforms, phosphorylation and role in neurodegenerative disorders, *Brain Res. Brain Res. Rev. 33*, 95−130.
2. Berriman, J., Serpell, L. C., Oberg, K. A., Fink, A. L., Goedert, M., and Crowther, R. A. (2003) Tau filaments from human brain and from in vitro assembly of recombinant protein show cross-beta structure, *Proc. Natl. Acad. Sci. U.S.A. 100*, 9034−9038.
3. LeVine, H., III (1993) Thioflavine T interaction with synthetic Alzheimer's disease beta-amyloid peptides: detection of amyloid aggregation in solution, *Protein Sci. 2*, 404−410.
4. Lee, V. M., Balin, B. J., Otvos, L., Jr., and Trojanowski, J. Q. (1991) A68: a major subunit of paired helical filaments and derivatized forms of normal Tau, *Science 251*, 675−678.
5. Schweers, O., Schonbrunn-Hanebeck, E., Marx, A., and Mandelkow, E. (1994) Structural studies of tau protein and Alzheimer paired helical filaments show no evidence for beta-structure, *J. Biol. Chem. 269*, 24290−24297.
6. Mena, R., Edwards, P. C., Harrington, C. R., Mukaetova-Ladinska, E. B., and Wischik, C. M. (1996) Staging the pathological assembly of truncated tau protein into paired helical filaments in Alzheimer's disease, *Acta Neuropathol. (Berlin) 91*, 633−641.
7. Galvan, M., David, J. P., Delacourte, A., Luna, J., and Mena, R. (2001) Sequence of neurofibrillary changes in aging and Alzheimer's disease: A confocal study with phospho-tau antibody, AD2, *J. Alzheimers Dis. 3*, 417−425.
8. Garcia-Sierra, F., Hauw, J. J., Duyckaerts, C., Wischik, C. M., Luna-Munoz, J., and Mena, R. (2000) The extent of neurofibrillary pathology in perforant pathway neurons is the key determinant of dementia in the very old. *Acta Neuropathol. (Berlin) 100*, 29−35.
9. Drubin, D. G., Feinstein, S. C., Shooter, E. M., and Kirschner, M. W. (1985) Nerve growth factor-induced neurite outgrowth in PC12 cells involves the coordinate induction of microtubule assembly and assembly-promoting factors, *J. Cell Biol. 101*, 1799−1807.
10. Khatoon, S., Grundke-Iqbal, I., and Iqbal, K. (1992) Brain levels of microtubule-associated protein tau are elevated in Alzheimer's disease: a radioimmuno-slot-blot assay for nanograms of the protein, *J. Neurochem. 59*, 750−753.
11. Zimmerman, S. B., and Trach, S. O. (1991) Estimation of macromolecule concentrations and excluded volume effects for the cytoplasm of *Escherichia coli*, *J. Mol. Biol. 222*, 599−620.
12. Chirita, C. N., Necula, M., and Kuret, J. (2003) Anionic Micelles and Vesicles Induce tau Fibrillization in vitro, *J. Biol. Chem. 278*, 25644−25650.
13. Hagihara, Y., Hong, D. P., Hoshino, M., Enjyoji, K., Kato, H., and Goto, Y. (2002) Aggregation of β_2-glycoprotein I induced by sodium lauryl sulfate and lysophospholipids, *Biochemistry 41*, 1020−1026.
14. Pertinhez, T. A., Bouchard, M., Smith, R. A. G., Dobson, C. M., and Smith, L. J. (2002) Stimulation and inhibition of fibril formation by a peptide in the presence of different concentrations of SDS, *FEBS Lett. 529*, 193−197.
15. Xiong, L. W., Raymond, L. D., Hayes, S. F., Raymond, G. J., and Caughey, B. (2001) Conformational change, aggregation and fibril formation induced by detergent treatments of cellular prion protein, *J. Neurochem. 79*, 669−678.
16. Garavito, R. M., and Ferguson-Miller, S. (2001) Detergents as tools in membrane biochemistry, *J. Biol. Chem. 276*, 32403−32406.
17. Carmel, G., Mager, E. M., Binder, L. I., and Kuret, J. (1996) The structural basis of monoclonal antibody Alz50's selectivity for Alzheimer's disease pathology, *J. Biol. Chem. 271*, 32789−32795.
18. Necula, M., Chirita, C. N., and Kuret, J. (2003) Rapid anionic micelle-mediated alpha-synuclein fibrillization in vitro, *J. Biol. Chem. 278*, 46674−46680.
19. Ksiezak-Reding, H., and Wall, J. S. (1994) Mass and physical dimensions of two distinct populations of paired helical filaments, *Neurobiol. Aging 15*, 11−19.
20. King, M. E., Ahuja, V., Binder, L. I., and Kuret, J. (1999) Ligand-dependent tau filament formation: implications for Alzheimer's disease progression, *Biochemistry 38*, 14851−14859.
21. Corrin, M. L., and Harkins, W. D. (1947) The Effect of Salts on the Critical Concentration for the Formation of Micelles in Colloidal Electrolytes. *J. Am. Chem. Soc. 69*, 683−688.
22. Maeda, H. (2001) Some Thoughts Regarding Theoretical Aspects of the Corrin-Harkins Relation and the Micellization Product of Ionic Micelles, *J. Colloid Interface Sci. 241*, 18−25.
23. Naiki, H., and Gejyo, F. (1999) Kinetic analysis of amyloid fibril formation, *Methods Enzymol. 309*, 305−318.
24. Nielsen, L., Khurana, R., Coats, A., Frokjaer, S., Brange, J., Vyas, S., Uversky, V. N., and Fink, A. L. (2001) Effect of environmental factors on the kinetics of insulin fibril formation: elucidation of the molecular mechanism, *Biochemistry 40*, 6036−6046.
25. Evans, K. C., Berger, E. P., Cho, C. G., Weisgraber, K. H., and Lansbury, P. T., Jr. (1995) Apolipoprotein E is a kinetic but not a thermodynamic inhibitor of amyloid formation: implications for the pathogenesis and treatment of Alzheimer disease. *Proc. Natl. Acad. Sci. U.S.A. 92*, 763−767.
26. Philo, R. D., and Selwyn, M. J. (1973) Use of progress curves to investigate product inhibition in enzyme-catalysed reactions. Application to the soluble mitochondrial adenosine triphosphatase, *Biochem. J. 135*, 525−530.
27. Newcombe, R. G. (1998) Improved confidence intervals for the difference between binomial proportions based on paired data, *Stat. Med. 17*, 2635−2650.
28. Chiu, Y. C., Han, Y. C., and Cheng, H. M. (1983) in *Structure/Performance Relationships in Surfactants*, *ACS Symposium Series 253* (Rosen, M. J., Ed.) pp 89−105, American Chemical Society, Washington, DC.
29. Tessari, M., Foffani, M. T., Mammi, S., and Peggion, E. (1993) Conformation and interactions of uteroglobin fragments 4-14 and 49-65 in aqueous solution containing surfactant micelles, *Biopolymers 33*, 1877−1887.
30. Wong, G. C., Tang, J. X., Lin, A., Li, Y., Janmey, P. A., and Safinya, C. R. (2000) Hierarchical self-assembly of F-actin and

cationic lipid complexes: stacked three-layer tubule networks, *Science 288*, 2035−2039.
31. Bales, B. L. (2001) A definition of the degree of ionization of a micelle based on its aggregation number, *J. Phys. Chem. B 105*, 6798−6804.
32. Quina, F. H., Nassar, P. M., Bonilha, J. B. S., and Bales, B. L. (1995) Growth of Sodium Dodecyl Sulfate Micelles with Detergent Concentration, *J. Phys. Chem. 99*, 17028−17031.
33. Soreghan, B., Kosmoski, J., and Glabe, C. (1994) Surfactant properties of Alzheimer's A beta peptides and the mechanism of amyloid aggregation, *J. Biol. Chem. 269*, 28551−28554.
34. Skutelsky, E., and Roth, J. (1986) Cationic colloidal gold--a new probe for the detection of anionic cell surface sites by electron microscopy, *J. Histochem. Cytochem. 34*, 693−696.
35. Pillot, T., Goethals, M., Vanloo, B., Talussot, C., Brasseur, R., Vandekerckhove, J., Rosseneu, M., and Lins, L. (1996) Fusogenic properties of the C-terminal domain of the Alzheimer beta-amyloid peptide, *J. Biol. Chem. 271*, 28757−28765.
36. Parente, R. A., Nir, S., and Szoka, F. C., Jr. (1990) Mechanism of leakage of phospholipid vesicle contents induced by the peptide GALA, *Biochemistry 29*, 8720−8728.
37. Nieva, J. L., Nir, S., Muga, A., Goni, F. M., and Wilschut, J. (1994) Interaction of the HIV-1 fusion peptide with phospholipid vesicles: different structural requirements for fusion and leakage, *Biochemistry 33*, 3201−3209.
38. Yokoyama, S., Obata, J., Fujie, T., and Nakagaki, M. (1993) Effect of Temperature on the Surface-Properties of Aqueous- Solution of Arachidonic-Acid. *Chem. Pharm. Bull. 41*, 6−11.
39. Schwartz, D. K., Viswanathan, R., Garnaes, J., and Zasadzinski, J. A. (1993) Influence of Cations, Alkane Chain Length, and Substrate on Molecular Order of Langmuir−Blodgett Films, *J. Am. Chem. Soc. 115*, 7374−7380.
40. King, M. E., Gamblin, T. C., Kuret, J., and Binder, L. I. (2000) Differential assembly of human tau isoforms in the presence of arachidonic acid, *J. Neurochem. 74*, 1749−1757.
41. Barghorn, S., and Mandelkow, E. (2002) Toward a unified scheme for the aggregation of tau into Alzheimer paired helical filaments, *Biochemistry 41*, 14885−14896.
42. Gamblin, T. C., King, M. E., Dawson, H., Vitek, M. P., Kuret, J., Berry, R. W., and Binder, L. I. (2000) In vitro polymerization of tau protein monitored by laser light scattering: method and application to the study of FTDP-17 mutants, *Biochemistry 39*, 6136−6144.
43. Gamblin, T. C., King, M. E., Kuret, J., Berry, R. W., and Binder, L. I. (2000) Oxidative regulation of fatty acid-induced tau polymerization, *Biochemistry 39*, 14203−14210.
44. Briehl, R. W., Mann, E. S., and Josephs, R. (1990) Length distributions of hemoglobin S fibers, *J. Mol. Biol. 211*, 693−698.
45. Wilson, D. M., and Binder, L. I. (1995) Polymerization of microtubule-associated protein tau under near-physiological conditions, *J. Biol. Chem. 270*, 24306−24314.
46. Greenberg, S. G., and Davies, P. (1990) A preparation of Alzheimer paired helical filaments that displays distinct tau proteins by polyacrylamide gel electrophoresis, *Proc. Natl. Acad. Sci. U.S.A. 87*, 5827−5831.
47. Shirahama, K. (1998) in *Polymer-surfactant systems* (Kwak, J. C. T., Ed.) pp 143−191, M. Dekker, New York.
48. Moroi, Y., Matuura, R., Kuwamura, T., and Inokuma, S. I. (1986) Anionic Surfactants with Divalent Gegenions of Separate Electric Charge − Solubility and Micelle Formation, *J. Colloid Interface Sci. 113*, 225−231.
49. Hill, T. L. (1963) *Thermodynamics of Small Systems*, Benjamin, New York,.
50. Reiter, J., and Epstein, I. R. (1987) Bimodality in the Cooperative Binding of Ligands to Molecules with Multiple Binding-Sites. *J. Phys. Chem. 91*, 4813−4820.
51. Shirahama, K., Kameyama, K., and Takagi, T. (1992) Bimodality in the Dodecylpyridinium Bromide Sodium Dextran Sulfate System as Observed by an Electrophoretic Method, *J. Phys. Chem. 96*, 6817−6820.
52. Kahlweit, M. (1982) Kinetics of Formation of Association Colloids, *J. Colloid Interface Sci. 90*, 92−99.
53. Jarrett, J. T., and Lansbury, P. T., Jr. (1993) Seeding "one-dimensional crystallization" of amyloid: a pathogenic mechanism in Alzheimer's disease and scrapie? *Cell 73*, 1055−1058.
54. Winnik, F. M., and Regismond, S. T. A. (1996) Fluorescence methods in the study of the interactions of surfactants with polymers, *Colloids Surf. A 118*, 1−39.
55. Blackley, H. K., Sanders, G. H., Davies, M. C., Roberts, C. J., Tendler, S. J., and Wilkinson, M. J. (2000) In-situ atomic force microscopy study of beta-amyloid fibrillization, *J. Mol. Biol. 298*, 833−840.
56. Scheibel, T., Kowal, A. S., Bloom, J. D., and Lindquist, S. L. (2001) Bidirectional amyloid fiber growth for a yeast prion determinant, *Curr. Biol. 11*, 366−369.
57. Goldsbury, C., Kistler, J., Aebi, U., Arvinte, T., and Cooper, G. J. (1999) Watching amyloid fibrils grow by time-lapse atomic force microscopy, *J. Mol. Biol. 285*, 33−39.
58. Wischik, C. M., Crowther, R. A., Stewart, M., and Roth, M. (1985) Subunit structure of paired helical filaments in Alzheimer's disease, *J. Cell Biol. 100*, 1905−1912.
59. Vogelsang, G. D., Zemlan, F. P., and Dean, G. E. (1990) Purification and solubilization of paired helical filaments from Alzheimer brains, *J. Neurochem. 54*, 148−155.
60. Perez, M., Valpuesta, J. M., Medina, M., Montejo de Garcini, E., and Avila, J. (1996) Polymerization of tau into filaments in the presence of heparin: the minimal sequence required for tau-tau interaction, *J. Neurochem. 67*, 1183−1190.
61. Goedert, M., Jakes, R., Spillantini, M. G., Hasegawa, M., Smith, M. J., and Crowther, R. A. (1996) Assembly of microtubule-associated protein tau into Alzheimer-like filaments induced by sulphated glycosaminoglycans, *Nature 383*, 550−553.
62. Friedhoff, P., Schneider, A., Mandelkow, E. M., and Mandelkow, E. (1998) Rapid assembly of Alzheimer-like paired helical filaments from microtubule-associated protein tau monitored by fluorescence in solution, *Biochemistry 37*, 10223−10230.
63. Friedhoff, P., von Bergen, M., Mandelkow, E. M., Davies, P., and Mandelkow, E. (1998) A nucleated assembly mechanism of Alzheimer paired helical filaments, *Proc. Natl. Acad. Sci. U.S.A. 95*, 15712−15717.
64. Ferrone, F. (1999) Analysis of protein aggregation kinetics, *Methods Enzymol. 309*, 256−274.
65. Kowalewski, T., and Holtzman, D. M. (1999) In situ atomic force microscopy study of Alzheimer's beta-amyloid peptide on different substrates: new insights into mechanism of beta-sheet formation, *Proc. Natl. Acad. Sci. U.S.A. 96*, 3688−3693.
66. Zhu, M., Souillac, P. O., Ionescu-Zanetti, C., Carter, S. A., and Fink, A. L. (2002) Surface-catalyzed amyloid fibril formation, *J. Biol. Chem. 277*, 50914−50922.
67. Brown, S. S., and Spudich, J. A. (1979) Nucleation of polar actin filament assembly by a positively charged surface, *J. Cell Biol. 80*, 499−504.
68. Ranganathan, R., Tran, L., and Bales, B. L. (2000) Surfactant- and salt-induced growth of normal sodium alkyl sulfate micelles well above their critical micelle concentrations, *J. Phys. Chem. B 104*, 2260−2264.
69. Stenberg, M., Werthen, M., Theander, S., and Nygren, H. (1988) A diffusion-limited reaction theory for a microtiter plate assay, *J. Immunol. Methods 112*, 23−29.
70. Bancher, C., Brunner, C., Lassmann, H., Budka, H., Jellinger, K., Wiche, G., Seitelberger, F., Grundke-Iqbal, I., Iqbal, K., and Wisniewski, H. M. (1989) Accumulation of abnormally phosphorylated tau precedes the formation of neurofibrillary tangles in Alzheimer's disease, *Brain Res. 477*, 90−99.
71. Biernat, J., Gustke, N., Drewes, G., Mandelkow, E. M., and Mandelkow, E. (1993) Phosphorylation of Ser262 strongly reduces binding of tau to microtubules: distinction between PHF-like immunoreactivity and microtubule binding, *Neuron 11*, 153−163.
72. Bramblett, G. T., Goedert, M., Jakes, R., Merrick, S. E., Trojanowski, J. Q., and Lee, V. M. (1993) Abnormal tau phosphorylation at Ser396 in Alzheimer's disease recapitulates development and contributes to reduced microtubule binding, *Neuron 10*, 1089−1099.
73. Alonso, A. C., Grundke-Iqbal, I., and Iqbal, K. (1996) Alzheimer's disease hyperphosphorylated tau sequesters normal tau into tangles of filaments and disassembles microtubules, *Nat. Med. 2*, 783−787.
74. Ruben, G. C., Ciardelli, T. L., Grundke-Iqbal, I., and Iqbal, K. (1997) Alzheimer disease hyperphosphorylated tau aggregates hydrophobically, *Synapse 27*, 208−229.
75. Alonso, A., Zaidi, T., Novak, M., Grundke-Iqbal, I., and Iqbal, K. (2001) Hyperphosphorylation induces self-assembly of tau into tangles of paired helical filaments/straight filaments, *Proc. Natl. Acad. Sci. U.S.A. 98*, 6923−6928.

76. Perry, G., Kawai, M., Tabaton, M., Onorato, M., Mulvihill, P., Richey, P., Morandi, A., Connolly, J. A., and Gambetti, P. (1991) Neuropil threads of Alzheimer's disease show a marked alteration of the normal cytoskeleton, *J. Neurosci. 11*, 1748−1755.
77. Turner, M. S., Briehl, R. W., Ferrone, F. A., and Josephs, R. (2003) Twisted protein aggregates and disease: the stability of sickle hemoglobin fibers, *Phys. Rev. Lett. 90*, 128103.
78. King, M. E., Ghoshal, N., Wall, J. S., Binder, L. I., and Ksiezak-Reding, H. (2001) Structural analysis of Pick's disease-derived and in vitro-assembled tau filaments, *Am. J. Pathol. 158*, 1481−1490.
79. Gray, E. G., Paula-Barbosa, M., and Roher, A. (1987) Alzheimer's disease: paired helical filaments and cytomembranes, *Neuropathol. Appl. Neurobiol. 13*, 91−110.
80. Kuret, J., Chirita, C., and Necula, M. (2002) Ligand-dependent inhibition and reversal of tau filament formation, *Neurobiol. Aging 23*, 999.

BI036034B